Superconductivity and metal to insulator transition in homogeneously disordered molybdenum thin films

Shilpam Sharma^{1*}, E. P. Amaladass¹, Neha Sharma², V. Harimohan¹, S. Amirthapandian³, Awadhesh Mani¹

¹Condensed Matter Physics Division, Materials Science Group, Indira Gandhi Centre for Atomic Research, Kalpakkam 603102, India

²Surface & Nanoscience Division, Materials Science Group, Indira Gandhi Centre for Atomic Research, Kalpakkam 603102, India

³Materials Physics Division, Materials Science Group, Indira Gandhi Centre for Atomic Research, Kalpakkam 603102, India

Disorder driven metal to insulator transition is reported in three dimensional thin films of molybdenum, deposited at room temperature using DC magnetron sputtering at different argon pressures. The disorder is tuned using deposition pressure as the sole parameter. A variation of particle sizes, room temperature resistivity and superconducting transition has been studied as a function of deposition pressure. The disordered molybdenum thin films are found to have large carrier concentration but very low mobility. Hall and conductivity measurements have been used to understand the effect of disorder on the carrier density and mobilities. Ioffe-Regel parameter is shown to correlate with the continuous metal-insulator transition in our samples.

Keywords: disordered thin films, metal-insulator transition, charge localization

I. Introduction

Even though an old avenue of research in material science, the studies on the effect of disorder on normal and superconducting states of metallic superconductors still remains an open problem that is enjoying a renewed interest recently [1-11]. The disorder and superconductivity have contrasting effects on the electrical properties of material: while the former causes increase in resistivity by localizing electron wave-functions, latter gives rise to zero resistivity on account of formation of long range ordered condensate in a macroscopic quantum state. Based on Bardeen-Cooper-Schrieffer (BCS) theory of *s*-wave superconductors, Anderson postulated that superconductivity in a metallic system can't be destroyed by weak or moderate disorder [12]. It was however, later observed that homogeneously disordered thin film of many s-wave superconductors show a superconductor to insulator transition (SIT) either with an increase in disorder tending towards strong disorder limit [5, 13-15] or under the application of magnetic field [16-18]. Two dimensional ultrathin films of many alloys like Mo-Ge, Mo-C and Nb-Si are reported to show SIT below a critical thickness [19-21]. A substantial theoretical work has also been done to understand the disorder driven many body quantum phase transitions [22, 23].

Normal state properties such as normal state resistivity and its temperature coefficient gets affected due to disorder in the material. For normal metals, disorder induced weak localization of charge carriers create discrete Anderson-localized states near the Fermi level [24] which upon increase in disorder give rise to a metal insulator transition (MIT). In addition, Coulomb interaction among electrons can open a gap at Fermi level and can cause MIT. The scaling theory of MIT in disordered metals incorporates both localization as well as electron interaction effects [25]. It predicts that in the case of 3D systems, the phase diagram can have at the most four phases, namely conventional metal, amorphous metal, critical and insulating phase. In the case of conventional metals, charge

transport is mainly controlled by electron-phonon interaction as described by Boltzmann transport where conductivity increases with decrease in temperature. In the amorphous metals, conductivity decreases with decreasing temperature but extrapolates to a finite zero temperature value in contrast to insulators where conductivity becomes zero at zero temperature.

In the superconducting phase, properties such as transition temperature (T_C), superconducting gap and upper critical field (H_{C2}) show strong dependence on the degree of disorder. Increasing disorder by reducing particle size is known to increase or decrease T_C and H_{C2} depending upon the coupling strength and the smearing of density of states at the Fermi level [26, 27]. Weakly coupled type I superconductors, such as Al, Sn, In, W and Re, show an increase in their T_C in the disordered state [26, 28, 29]. Type II superconductor with intermediate coupling like Nb shows a decrease in the superconducting gap and T_C with reduction in particle size [30]. For strongly coupled Pb, while many reports on thin films exhibit no size dependent change in T_C [29], there is a report of reduction in T_C of Pb powder with grains below a critical size mainly due to discretization of electronic energy levels [31].

Disordered thin films of weakly coupled, type-I superconductor molybdenum (Mo) are reported to show an enhanced T_C as high as 6.7 to 8 K [26, 27]. Its T_C in crystalline bulk form is 915 mK and critical field \sim 98 Oe [32-35]. Reports on the effect of stress, morphology, size and dimensionality on the superconducting properties of Mo thin films show that T_C increases marginally with increase in stress [36, 37] and is correlated with sheet resistance [38] and residual resistivity ratio.

Almost all the reports of enhancement of T_C in thin Mo films are based on studies on quench-condensed two dimensional films deposited at liquid helium temperature [38]. In this paper, we report disorder induced SIT observed in three dimensional (3D) molybdenum thin films, sputter

deposited at room temperature under varying argon pressure. In addition to transition into insulating state, our homogeneously disordered thin films show enhancement in T_C as reported in amorphous Mo films [26]. A detailed structural characterization and analysis using high resolution transmission electron microscopy (HRTEM) have been performed to understand the effect of deposition pressure on the normal state resistivity and grain size. Effective disorder in these films has been characterized by the Ioffe-Regel parameter ($k_F l$) [39] that varies between $k_F l \sim 0.08$ -3.8 for our samples (k_F is the Fermi wave vector and l_e is the electron mean free path). A striking correlation in deposition pressure, disorder and particle size with superconducting and normal state properties of the Mo films has been brought about from these analysis. The change in $k_F l$ correlates with the change in average particle size and room temperature resistivity of homogeneously disordered thin films. One of the important aspect of current study is that the morphology and disorder could be reproducibly tuned by varying only the argon pressure during deposition of thin films.

II. Experimental Details

Homogeneously disordered nano-crystalline thin films of Mo were deposited on the cleaned glass substrates using a home built magnetron deposition system. Sputter deposition was carried out from a 99.97% pure Mo target using a custom built 1" magnetron cathode. Deposition chamber can reach up to a base pressure of $\sim 3x10^{-7}$ mbar and oxygen partial pressure measured using residual gas analyzer was found to be less than 10^{-9} mbar. The average particle size in the Mo films was reproducibly controlled by varying Ar pressure in 13 µbar to 3 µbar range. This pressure range is much lower than the deposition pressures used by Sangita et al. [40] to achieve smaller particle sizes in sputter deposited Nb films. Films were deposited with direct current fixed at 40 mA and voltage varying between 270 V and 325 V. Thickness measurements were performed using Dektak

profilometer, Rutherford back scattering and X-ray reflectivity (XRR) measurements. As the films were found to be X-ray amorphous, phase and microstructure of the nano-crystalline films was characterized using transmission electron microscopy (TEM) on mechanically scratched films transferred onto carbon grid. High resolution TEM measurements were performed using LIBRA 200FE HRTEM operated at 200 keV, equipped with an in-column energy filter and Schottky field emission gun source. Electron diffraction patterns (SAED) and electron energy loss spectrums (EELS) were collected at different regions of the samples to confirm purity of Mo phase in the films. In-field transport measurements were performed using M/S cryogenic Inc. U.K. make cryogen free, 15 T magneto-transport cryostat capable of reaching temperatures as low as 1.8 K from 300 K. Hall and resistivity measurements were performed in Hall bar and Van der Pauw geometry respectively [41, 42].

III. Results and Discussion

All the nano-crystalline Mo films were deposited on glass substrates at different Ar pressures varying from 3 μ bar to 13 μ bar while maintaining same DC current of 40 mA. The thickness of all the films was found to be roughly 56 nm as measured using Rutherford backscattering, Dektak profilometer and XRR measurements.

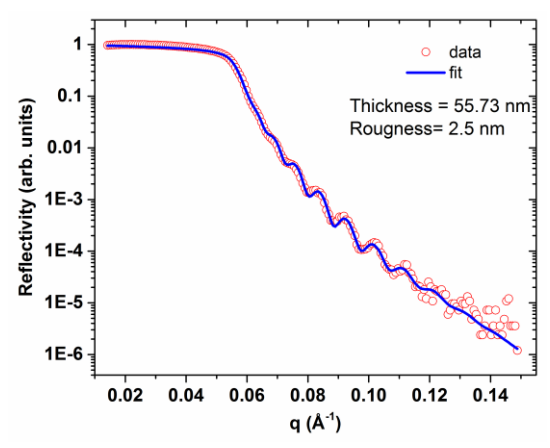


Figure 1: X-ray reflectivity as a function of scattering vector. Thickness of film was estimated by fitting the XRR data. A thickness of ~56 nm with a low surface roughness of ~2.5 nm has been observed.

To estimate film thickness and roughness, XRR data was fitted using Parratt32 routine [43]. A representative XRR data along with fitting is presented in figure 1. The surface roughness of the films was found to be ~2.5 nm. These Mo thin films were characterized for phase and microstructure using HRTEM. Figure 2(a)-(d) show the HRTEM images of the films deposited at different Ar pressures 3.0, 4.5, 7.0 and 13.0 μbar respectively. It can be clearly seen that the film deposited at 3 μbar has large particles with sharp particle boundaries and as the deposition pressure increases, particle sizes reduces. In the HRTEM image (c.f. Figure 2(e)) of sample deposited at 3 μbar Ar pressure, two grains can be identified with crystalline order ranging up to 5-6 nm with inter-granular region of roughly 2 nm. With increase in deposition pressure, inter-granular region comprising of amorphous Mo with no long range order but some degree of short range order is seen to increase.

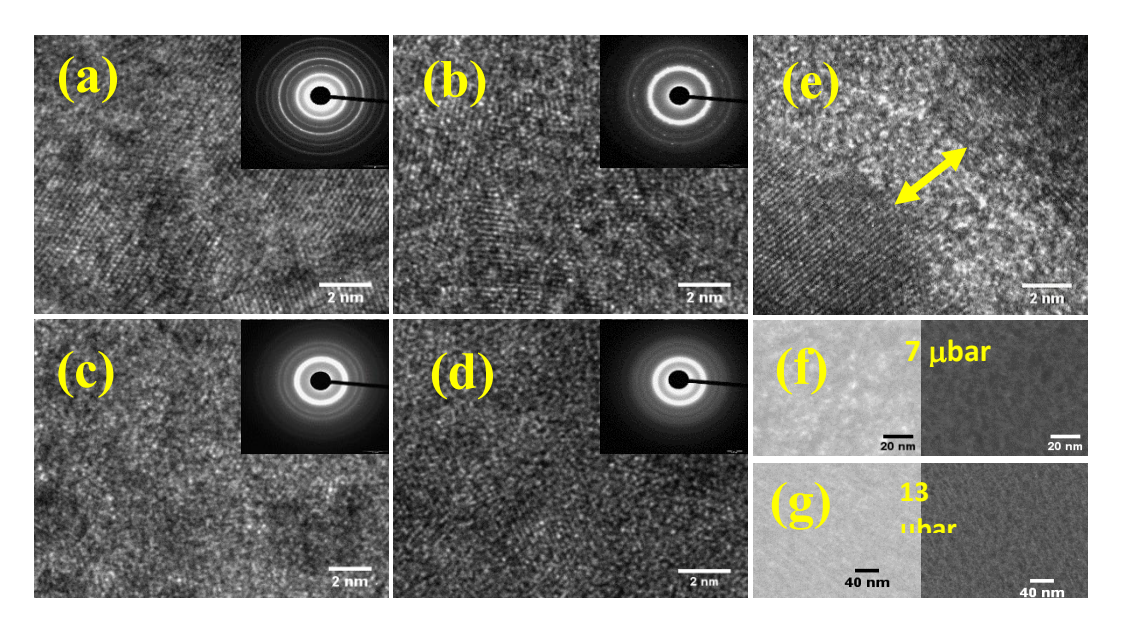


Figure 2 (a-d): HRTEM images of Mo thin films deposited at Ar pressure 3.0, 3.5, 4.5, 5.5 μbar respectively. Grain size reduces and inter-granular region with short range order increases with increase in deposition pressure. SAED patterns of samples deposited at different pressures show a change of polycrystalline ring pattern to diffused ring pattern typical of amorphous materials. (e): shows intergrain region of around 2 nm between grains having long range order up to 5-6 nm. (f)-(g): bright field and dark field images for samples deposited at 7 and 13 μbar pressure shows that the particle density reduces with increase in deposition pressure.

Figure 2(a)-(d) also show SAED patterns taken at different regions of sample. It can be observed from figure 2(a) that the film deposited at 3 µbar is polycrystalline in nature with well-defined Debye-Scherrer ring pattern. The ring pattern was analyzed using "processdiffraction' software [44]. All the d-spacing in SAED pattern were indexed to BCC Mo with a lattice parameter ~2.9404 Å, smaller than the reported value of 3.1472 Å [45] thus indicating a compressive stress in the film. Similar changes in lattice parameters of nano-crystalline films of Nb and gold have already been reported in literature [30, 46, 47]. Other than BCC Mo d-spacings, the d-spacing corresponding to impurity phases like molybdenum oxide etc. have not been observed in the diffraction pattern. With increase in the deposition pressure, Debye-Scherrer rings in the SAED patterns (c.f. figure 2b-d) can't be discerned and the patterns resemble diffraction pattern of amorphous material with diffused rings. For sample deposited at 4.5 µbar pressure (figure 2(b)), a few crystalline spots can be observed on the amorphous electron diffraction pattern. Figure 2(f) and 2(g) show dark field and bright field TEM micrographs for 7 µbar and 13 µbar deposited samples. Dark contrast due to diffracting grains can be observed. It is seen that the number density of the particles is decreasing with increase in deposition pressure.

The particle size distribution of these films has been estimated by analyzing dark field TEM micrographs using ImageJ software [48]. The average particle size has been estimated by fitting log-normal distribution to the size distribution histograms of roughly 100-150 different particles. The particle size distribution along with a representative dark field TEM micrograph is presented in figure 3. The average particle size decreases from 5.5 nm to 2.5 nm with increase in deposition pressure (P) from 3 μ bar to 7 μ bar. With a further increase of pressure from 7 μ bar to 13 μ bar, particle size does not decrease below ~2.5 nm, nonetheless, the average particle density decreases for the films deposited in this pressure range. The variation of average particle size with deposition

pressure is presented in figure 4. It can be seen that particle size decreases rapidly as the pressure is increased from 3 μ bar to 7 μ bar and beyond P > 7 μ bar it remains nearly constant at ~2.5 nm. Nano-structured Nb thin films deposited at same Ar pressure were reported to have ~60 nm particles and the smallest particle of ~5 nm for 13 μ bar deposition pressure [40]. In addition, for Nb films particle size was not solely dependent upon deposition pressure [40] but substrate temperature and DC power were also adjusted to obtain a particular particle size. In our Mo thin films a reproducible and nearly linear decrease of particle size with deposition pressure up to 7 μ bar has been observed beyond which particle size saturates. A smaller value of lattice parameter seen in our film can be due to pressure from grain boundary on these small crystallites.

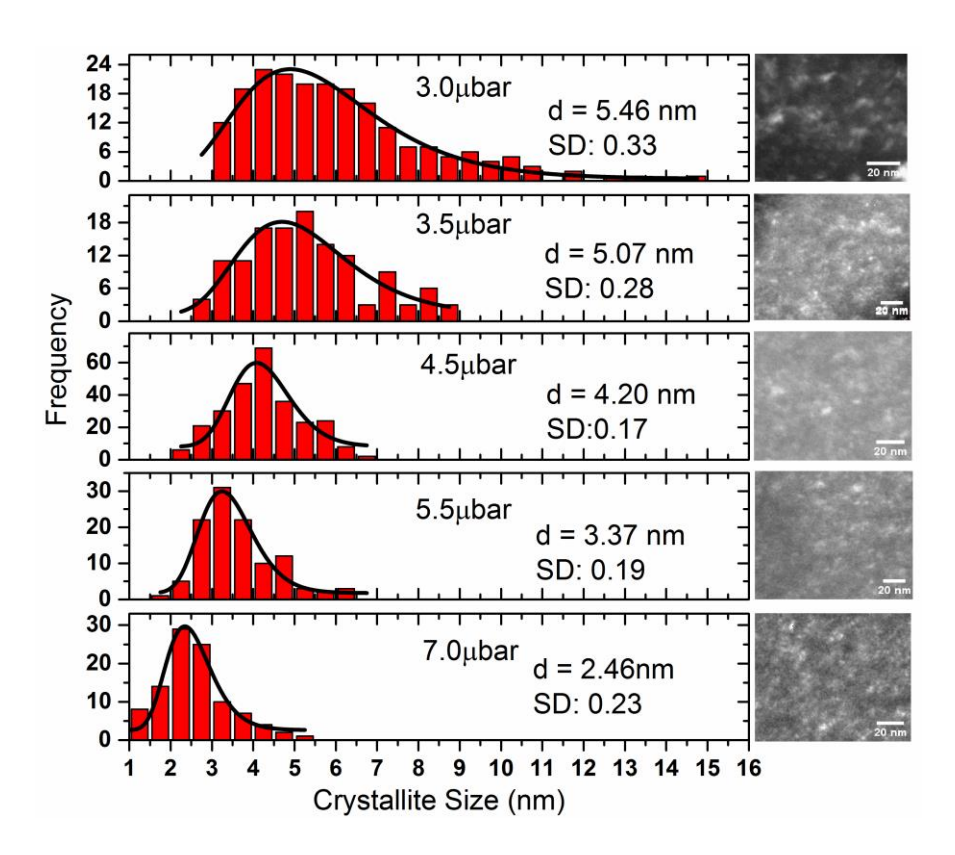


Figure 3: Particle size distribution in Mo thin films deposited at different Ar pressures from 3.0 to 7.0 μbar. A decrease in particle size is observed with increase in deposition pressure. Figure also presents dark field TEM micrographs of the corresponding thin films used to deduce particle sizes.

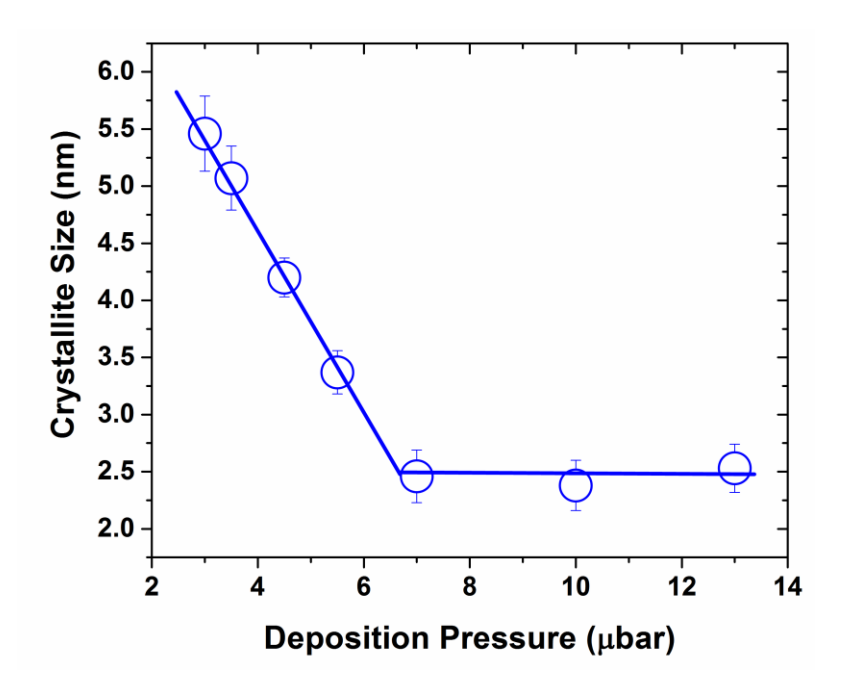


Figure 4: Variation of average particle size with deposition pressure. A quick fall in particle size is observed when deposition pressure was increased from 3 μ bar to 7 μ bar. Above 7 μ bar the particle size remains constant at ~2.5 nm. Blue lines are for guidance.

Figure 5 shows temperature variation of resistance normalized with resistance at 299 K. Superconducting transition is found to occur in samples with particle sizes up to 3.4 nm (i.e. films deposited up to $P = 5.5 \mu bar$). Resistive transitions to the superconducting state are shown in inset (a) of figure 5. T_C is well defined and much higher than bulk $T_C \sim 915$ mK, thus providing evidence of homogeneous disorder in our Mo thin films. Variation of T_C with pressure along with respective particle size is shown in inset (b) of figure 5. A dome shaped variation of T_C is seen with maximum at ~ 5.5 K occurring for the film with 4.2 nm particle size deposited at 4.5 μ bar pressure. This non-monotonic variation of T_C with deposition pressure or particle size can be understood as follows. T_C decreases for films deposited at higher pressure ($P > 4.5 \mu$ bar) due to increase in disorder and localization of carriers, on the other hand, for the films deposited at lower pressure ($P < 4.5 \mu$ bar) since the crystallinity increases with decreasing pressure, the T_C starts decreasing from its

maximum value in disordered state to finally approaching towards its bulk value in crystalline Mo. Moreover, in contrast to report by Fabrega et al. [36], the $T_{\rm C}$ of our superconducting films is found to be independent of their thickness.

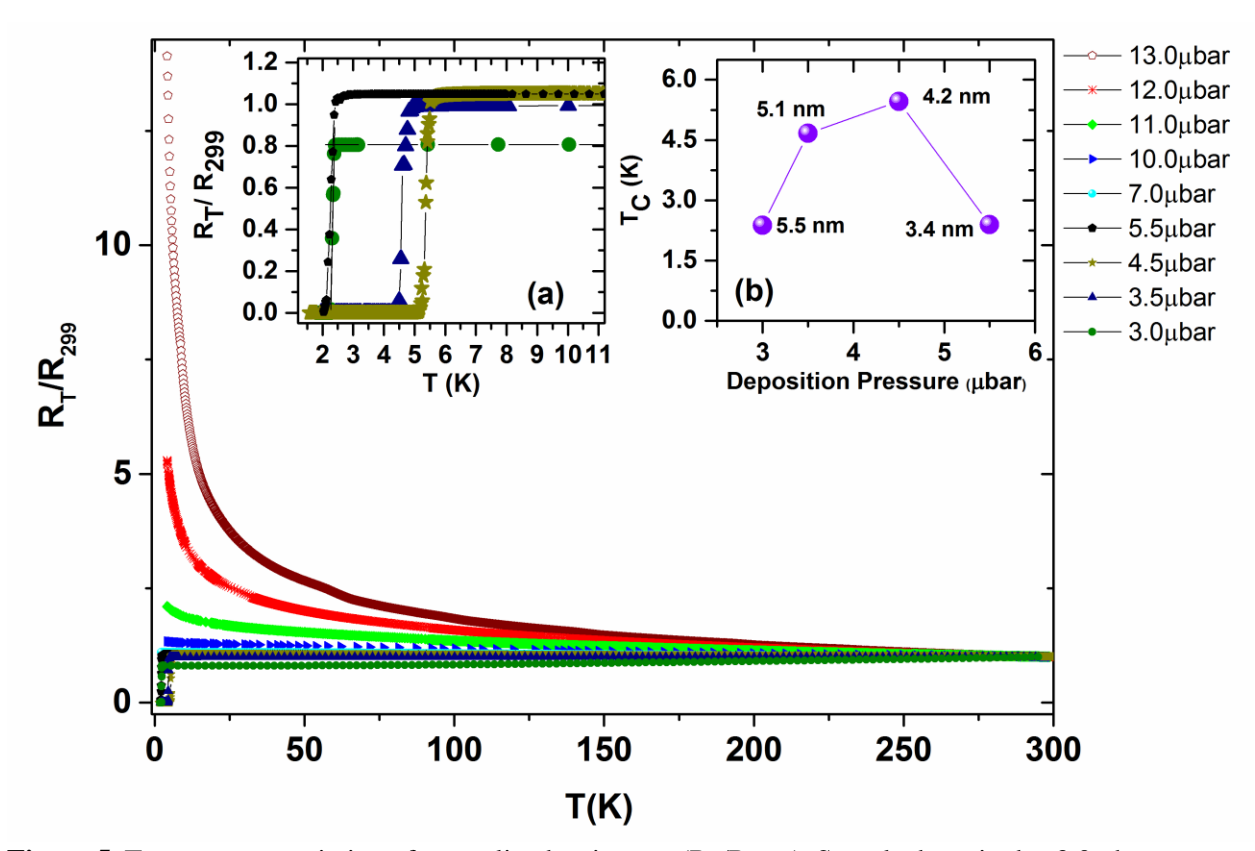


Figure 5: Temperature variation of normalized resistance ($R_T/R_{299\,K}$). Sample deposited at 3.0 µbar pressure shows positive TCR. **Inset (a):** superconducting transitions at different temperatures do not show re-entrant behavior. **Inset (b):** Variation of T_C with deposition pressure and particle size. T_C shows an increase up to 5.5 K for sample deposited at 4.5 µbar pressure. Above this pressure, T_C again reduces with no superconductivity down to 2 K for sample deposited at 7.0 µbar.

As evident from figure 5, upon increasing the deposition pressure, a change in the temperature coefficient of resistance (TCR) has been observed. Film with average particle size ~5.5 nm (deposited at $P=3~\mu bar$) shows positive TCR with a residual resistivity ratio (RRR = $R_{299~K}/R_{6~K}$) of ~1.2, whereas a RRR ~1 has been observed for the sample deposited at $P=3.5~\mu bar$ with little temperature dependence of normal state resistivity up to superconducting transition. Films

deposited at $P \ge 4.5$ µbar showed negative TCR with RRR as low as 0.07. A plot of RRR for all the films with respect to deposition pressure is presented in figure 6. RRR decreases monotonically with increase in deposition pressure but the rate of decrease of RRR becomes larger for the films deposited at P > 7 µbar.

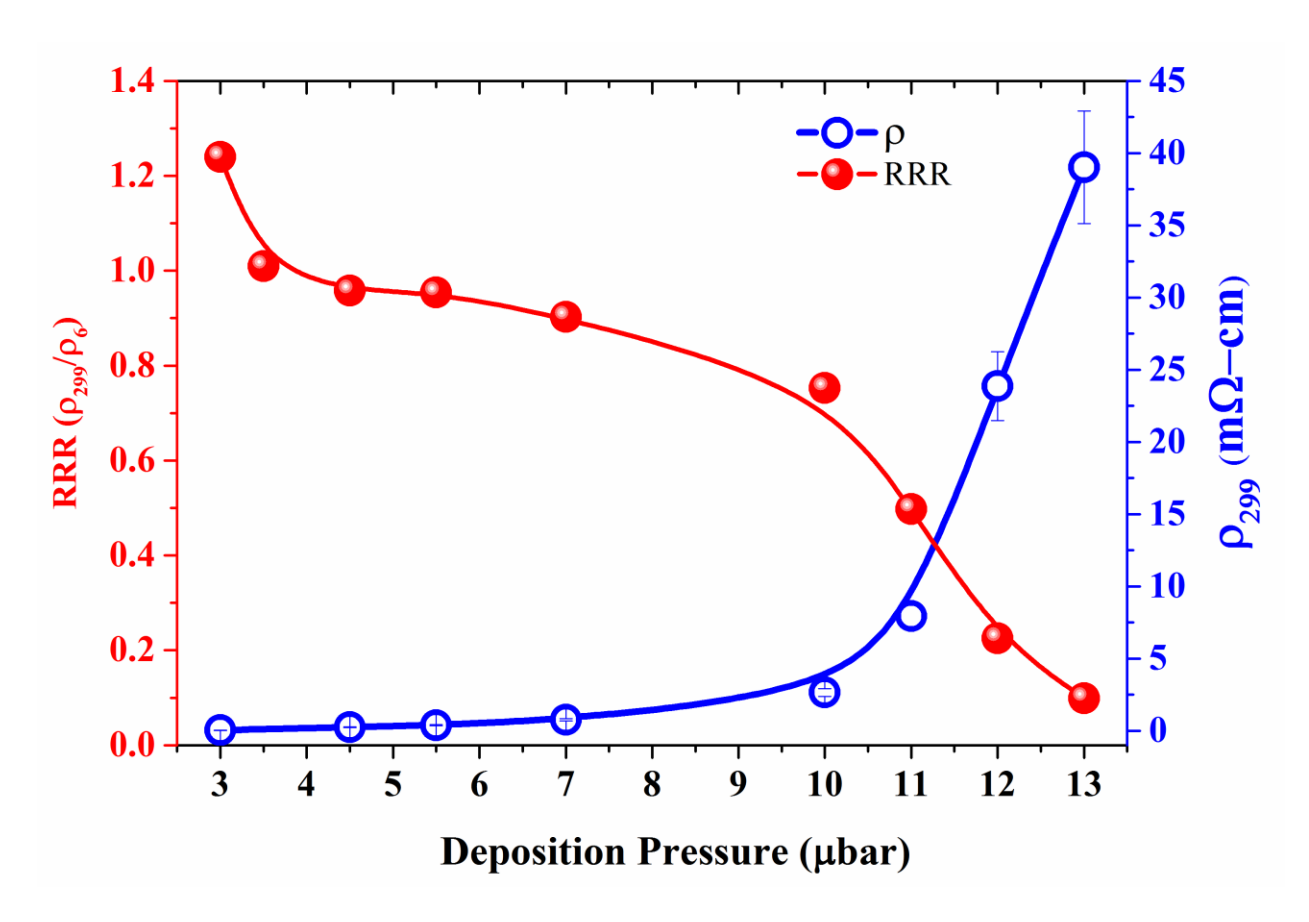


Figure 6: Variation of room temperature resistivity and RRR as a function of deposition pressure. The increase in room temperature resistivity is small up to 7 μ bar and it increases faster for samples deposited at further higher pressures.

Variation of room temperature resistivity (ρ_{299}) of these thin films as a function of deposition pressure is also presented in figure 6. A slow increase in room temperature resistivity was observed for samples deposited up to P=7 µbar pressure, beyond which room temperature resistivity increases rapidly. A comparison with variation of particle size as a function of deposition pressure (cf. figure 4) reveals that the resistivity increases slowly when particle size decreases rapidly from

5.5 nm to 2.5 nm but then increases rapidly in the range where particle size remains constant at 2.5 nm. This observation indicates that the variation in resistivity can't be explained on the basis of particle size and dimensions as reported by Fabrega et al. [36].

To understand a rapid increase in the resistivity of Mo films deposited at P > 7 µbar, Ioffe-Regel parameter $(k_F l)$ which characterize the disorder was calculated from room temperature (299 K) Hall coefficient and resistivity. Here k_F is the Fermi wave vector and l is the electronic mean free path. Ioffe-Regel criterion describes transition of a metal into an insulator primarily due to increased disorder and reduced carrier density. Electrons in a metal localizes when the mean free path reduces below Fermi wave vector and the system can transition into a weak insulating phase that remains fairly conducting at any finite temperatures. In a non-interacting system with free electrons, $k_F l$ offers a distinctive measure of electronic disorder. This however is not true in a dielectric state where electron-electron (e-e) interactions cannot be ignored. Thus the $k_F l$ calculations were performed from Hall coefficient and resistivity measured at room temperature, where e-e interaction effects are not very large. Ioffe-Regel parameter was calculated using the free electron formula $k_F l = \left\{ (3\pi^2)^{\frac{2}{3}} \hbar R_H^{\frac{1}{3}} \right\} / [\rho e^{5/3}]$ (\hbar is Planck's constant, R_H is Hall coefficient, ρ is resistivity and e is the electronic charge) [39]. Hall measurements were performed on samples deposited in Hall bar geometry. A standard four probe AC technique using lock-in amplifier to record transverse resistances (R_{xy}) as a function of magnetic field has been used. The Hall resistance as a function of magnetic field for samples deposited at different deposition pressures is presented in figure 7. A positive slope of R_{xy} (B) plots indicate that holes are the dominant carriers. It is already reported [49] that Mo is a compensated metal with holes having higher mobility ($\mu_h \sim 2\mu_e$ at 300 K) than electrons and thus shows positive Hall voltage.

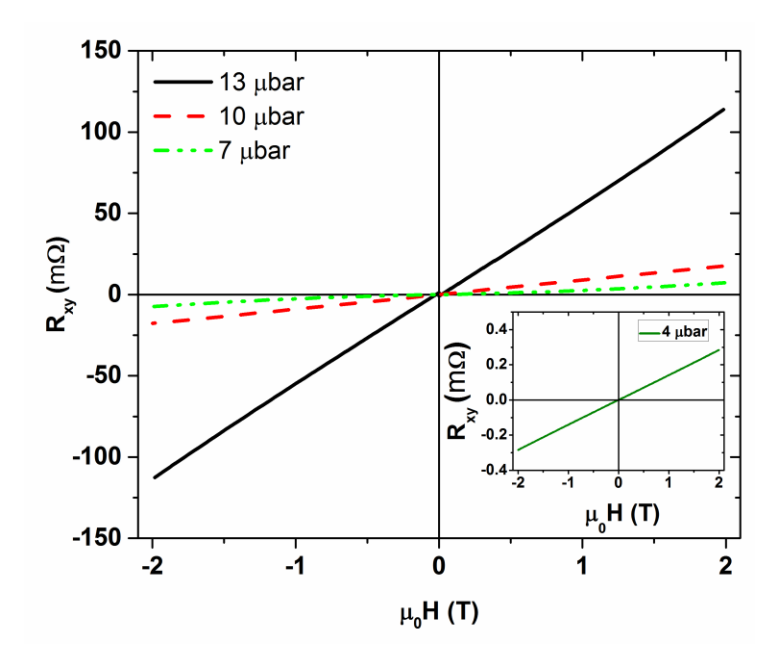


Figure 7: The Hall (transverse) resistance as a function of magnetic field for samples deposited at different deposition pressures. A positive slope of R_{xy} (B) plots indicate that holes are the dominant carriers. The data is presented after subtracting the longitudinal resistance of the samples.

Variation of Hall coefficient as a function of deposition pressure is shown in inset (a) of figure 8. Hall coefficient increases with increase in deposition pressure. This could be due to decrease in mobility of charge carriers or decrease in the number of charge carriers taking part in conduction. The value of Hall coefficient in our disordered Mo films is very close to the value reported for 30 nm thick amorphous Mo film [49, 50]. It could be observed from inset (b) of the figure 8 that while mobility of charge carrier does not change much, the charge carriers shows a decrease by two orders of magnitude with increase in deposition pressure. This indicates charge carrier localization in the disordered samples. The charge carrier concentration varies between 10^{27} to 10^{29} m⁻³ which is consistent with the reported value [50]. Even though we find a high carrier concentration in our samples, the mobility $\sim 10^{-1}$ cm²/V-sec. is several orders of magnitude lower than that of metals

or semiconductors and in particular from that of Mo metal [49]. These low values of charge mobility are commensurate with the assertion of the high degree of disorder in our samples.

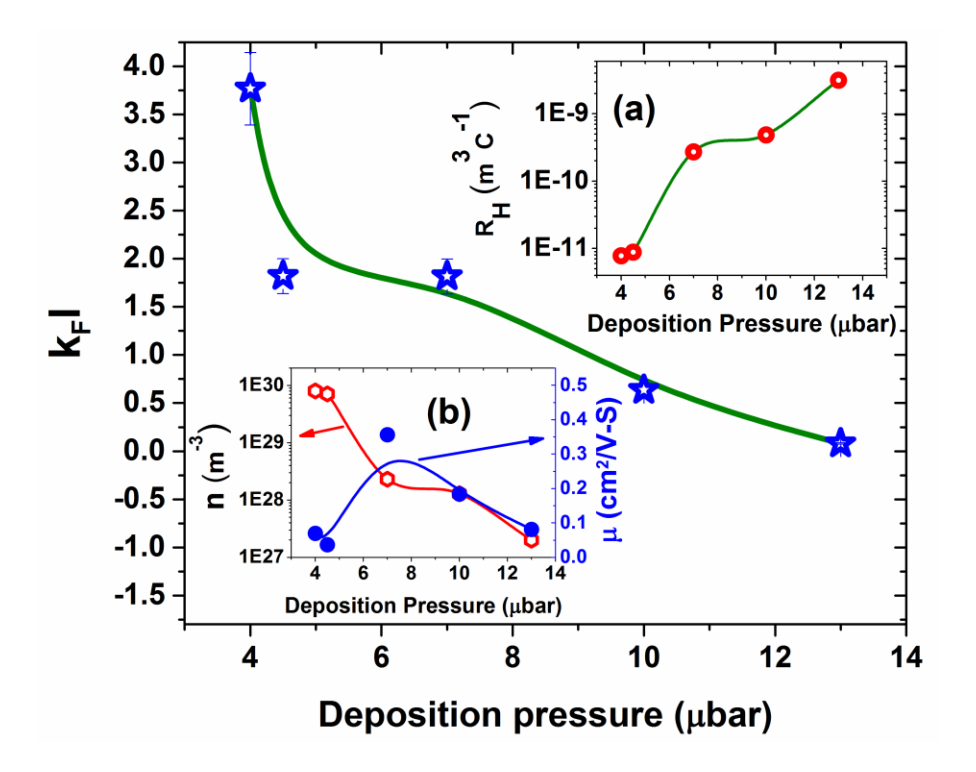


Figure 8: Ioffe-Regel parameter plotted as a function of deposition pressure. $k_F l$ shows a monotonous decrease with increase in deposition parameter. The value of $k_F l$ is >1 for samples deposited at $P \le 7$ μbar. MIT occurs for samples having $k_F l < 1.0$ deposited at $P \ge 10$ μbar Inset (a): Plot of R_H vs. deposition pressure shows an increase in Hall coefficient with increase in pressure. Inset (b): variation of charge carrier density and mobility as a function of deposition pressure. It is evident that the carrier density is reducing by increasing deposition pressure indicating a disorder driven localization. The mobility is seen to be several orders of magnitude less than that in conventional metals but is found to be independent of the deposition pressure.

Main panel of figure 8 shows variation of $k_F l$ as a function of deposition pressure. With increase in deposition pressure, $k_F l$ decreases monotonically from ~3.8 to 0.08. As can be seen from figure 8, the films deposited at pressures between 3-7 µbar have $k_F l > 1$, whereas, kF l < 1 for films deposited at $P \ge 10$ µbar. Thus all the samples deposited at pressures higher than 10 µbar become

weakly insulating due to disorder induced charge carrier localization as per the Ioffe-Regel criterion.

To substantiate the existence of insulating state in samples having $k_F l < 1$, an analysis of the logarithmic derivative of conductivity (σ) as a function of temperature has been performed based on the technique introduced by Mobius et al. [51, 52]. The plot of mathematical function w(T) = $\frac{d \ln \sigma}{d \ln T}$ shows distinctively different behavior for insulating and metallic films. While the w(T) plot diverges to infinity as the temperature is reduced for an insulating sample, it extrapolates to zero at zero temperature for metallic samples. The function w(T) has been calculated using linear regression fit of $\ln \sigma$ vs. $\ln T$ plots. Plots of w(T) as a function of $T^{1/2}$ for samples deposited at different pressures are shown in figure 9a. It can be observed that the w(T) values for samples deposited up to 7 µbar pressure appear to extrapolate to zero with decrease in sample temperature. This downward trend at low temperature is a manifestation of metallic or amorphous metals. The samples deposited at P > 10 µbar show an upward trend in their w(T) plots with reduction in temperature which gives a clear evidence of existence of localized insulating state [53] in these samples. From the plots of w(T) it is now reasonably clear that there is a metal to insulator transition occurring in samples deposited between 7 µbar and 10 µbar pressure. This explains the rapid rise in room temperature resistivity for samples deposited at $P \ge 10 \mu bar$, even though particle size remains nearly the same for these samples. A similar observation of MIT in highly disordered RuO₂ films having very large carrier concentrations and very low mobilities has recently been reported [10].

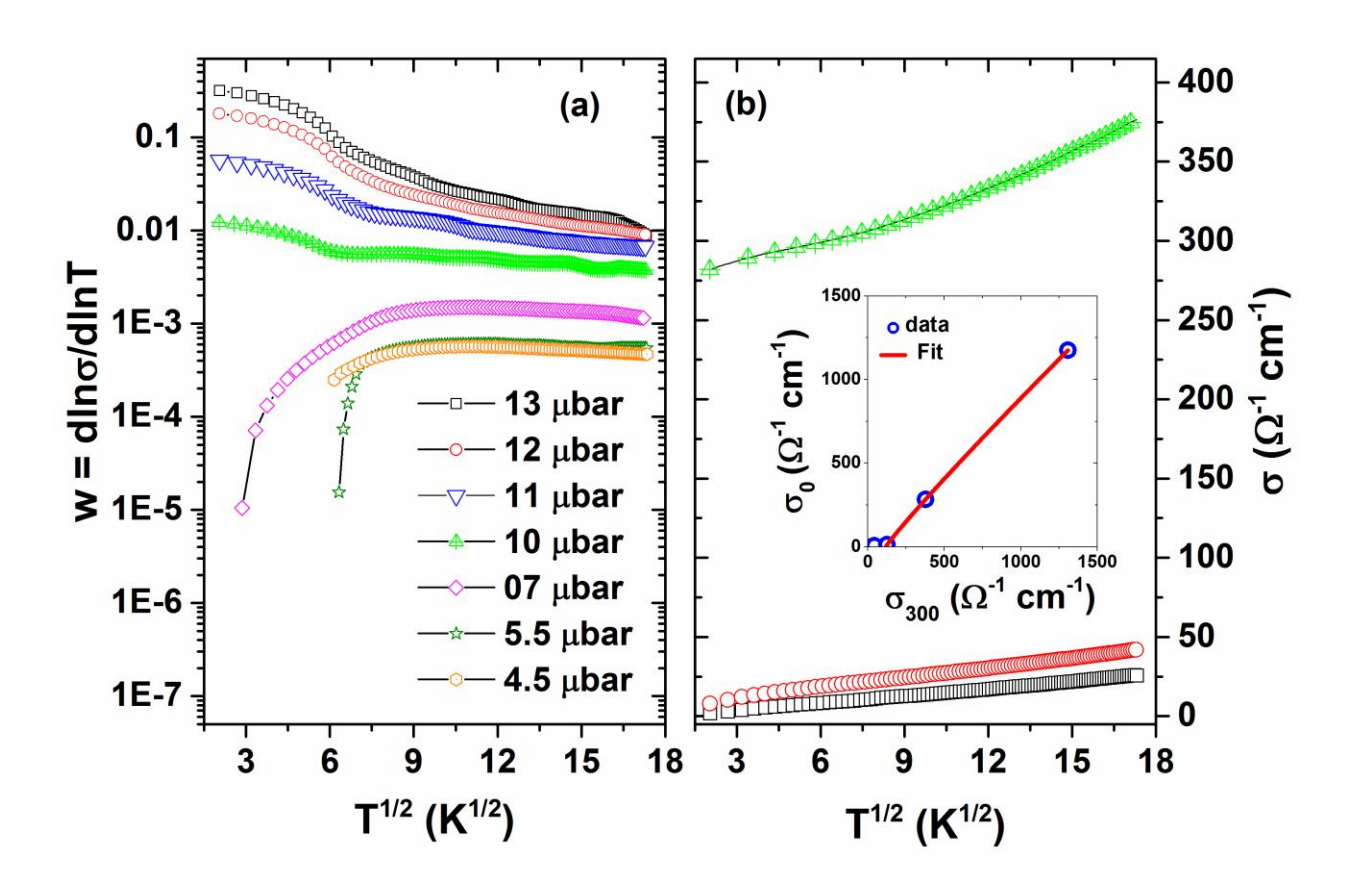


Figure 9a: Plot of logarithmic derivative of conductivity as a function of temperature shows a metal-insulator transition occurring in disordered Mo films. Samples deposited at $P \le 7$ μbar show amorphous metallic character and the samples deposited at $P \ge 10$ μabr show weakly localized insulating phase. **Figure 9(b):** Plot of conductivity as a function of $T^{1/2}$ show that the films are three dimensional disordered systems with slopes ranging between 1.5 to 7.6 (Ω cm)⁻¹K^{-1/2}. **Inset:** Shape of mobility edge and its fitting show that a continuous three dimensional metal-insulator transition occurs beyond critical conductivity of 117 (Ω cm)⁻¹.

In the case of disordered 3D metals, having weakly localized charge carrier transport with enhanced electron-electron interactions, the conductivity shows a temperature dependence of the form $\sigma = \sigma_0 + \sigma_1 T^{\upsilon}$, ($\nu = \frac{1}{2}$ for 3D disordered case) [25, 54, 55]. The plots of $\sigma(T)$ were fitted to above equation keeping the temperature exponent ν both as variable and fixed at $\frac{1}{2}$. The fitted exponent ν ranged between 1.2 for sample deposited at P = 7 µbar to ~0.5 for samples deposited at P > 10 µbar pressure. The value of $\nu \sim 0.5$ for our samples indicate that the samples are three dimensional disorderd thin films. Figure 9b shows the variation of conductivity as a function of

 $T^{1/2}$. The slopes of the $\sigma(T^{1/2})$ plots varies between 1.5 (Ω cm)⁻¹K^{-1/2} for sample deposited at 13 µbar and 7.6 (Ω cm)⁻¹K^{-1/2} for sample deposited at 10 µbar that shows weakly localized phase. This value of slope for sample near the MIT is consistent with the similar reports of MIT in 3D disordered samples [25, 55].

The slope of mobility edge is a very important parameter in understanding MIT in disordered metals. In three dimensions, it is defined as a relationship between zero temperature conductivity (σ_0) and a driving parameter generally taken as bare conductivity. Bare conductivity is usually approximated by room temperature conductivity (σ_{300}) [55]. The σ_0 values have been determined by fitting $\sigma(T)$ data with above given equation while keeping v = 1/2. The shape of the mobility edge has been obtained by plotting σ_0 as a function of room temperature conductivity of the samples. Inset of figure 9b shows the shape of mobility edge for our disordered Mo films. The points are fitted to $\sigma_0 = A (\sigma_{300} - \sigma_c)^{\beta}$, where σ_c is the room temperature critical conductivity at the transition and β is critical exponent having a value ~1 for disordered metals [54]. The fit is shown in the inset of figure 9b. The value of β is found to be 0.94 which is consistent with the reported values for MIT in other disordered metals [55]. The room temperature critical conductivity has been found to be 117 (Ω cm)⁻¹.

IV. Conclusion

In conclusion, we have shown that the homogeneously disordered thin films of molybdenum exhibit superconductivity at higher transition temperature than the bulk and their T_C depends upon the degree of disorder in the films. The superconducting transition and normal state properties of these disordered thin films could be reproducibly tuned just by varying Ar pressure during deposition. An increase in T_C of Mo thin films was previously reported only in quench condensed

amorphous Mo thin films, where alloying was required to stabilize higher T_C at room temperature [26, 27]. In present study, a large increase in the T_C of room-temperature-deposited Mo thin films has been observed which remains stable even with thermal cycling to low temperatures.

The films show a metal to insulator transition with increase in the disorder due to localization of charge carriers. The carrier density of Mo films is seen to decrease with increase in the disorder. The mobility of charge carrier has been found to be 3-4 orders of magnitude less than that of the metals. The analysis of Ioffe-Regel parameter and conductivity data clearly indicates that the films are three dimensional disordered systems which undergo a continuous metal-insulator transition.

Acknowledgements

The authors would like to thank Dr. B. Sundaravel, Materials Science Group, IGCAR for Rutherford backscattering measurements and estimation of film thickness. Authors would also like to thank Dr. Sanjay Rai, RRCAT, Indore for X-ray reflectivity measurements. The authors gratefully acknowledge UGC-DAE-CSR node at Kalpakkam for providing access to the 15 T cryogen free magneto-resistance set up and high resolution TEM imaging.

References

- [1] Ghosal A, Randeria M and Trivedi N 1998 Role of Spatial Amplitude Fluctuations in Highly Disordered s-Wave Superconductors *Physical Review Letters* **81** 3940-3
- [2] Mondal M, Kamlapure A, Chand M, Saraswat G, Kumar S, Jesudasan J, Benfatto L, Tripathi V and Raychaudhuri P 2011 Phase Fluctuations in a Strongly Disordered s-Wave NbN Superconductor Close to the Metal-Insulator Transition *Physical Review Letters* **106** 047001
- [3] Mondal M, Chand M, Kamlapure A, Jesudasan J, Bagwe V, Kumar S, Saraswat G, Tripathi V and Raychaudhuri P 2011 Phase Diagram and Upper Critical Field of Homogeneously Disordered Epitaxial 3-Dimensional NbN Films *J Supercond Nov Magn* **24** 341-4
- [4] Kamlapure A, Das T, Ganguli S C, Parmar J B, Bhattacharyya S and Raychaudhuri P 2013 Emergence of nanoscale inhomogeneity in the superconducting state of a homogeneously disordered conventional superconductor *Sci. Rep.* **3:2979**
- [5] Chand M, Saraswat G, Kamlapure A, Mondal M, Kumar S, Jesudasan J, Bagwe V, Benfatto L, Tripathi V and Raychaudhuri P 2012 Phase diagram of the strongly disordered *s*-wave superconductor NbN close to the metal-insulator transition *Physical Review B* **85** 014508

- [6] Kowal D and Ovadyahu Z 2008 Scale dependent superconductor—insulator transition *Physica C:* Superconductivity **468** 322-5
- [7] Sherman D, Kopnov G, Shahar D and Frydman A 2012 Measurement of a Superconducting Energy Gap in a Homogeneously Amorphous Insulator *Physical Review Letters* **108** 177006
- [8] Dubi Y, Meir Y and Avishai Y 2007 Nature of the superconductor-insulator transition in disordered superconductors *Nature* **449** 876-80
- [9] Sherman D, Gorshunov B, Poran S, Trivedi N, Farber E, Dressel M and Frydman A 2014 Effect of Coulomb interactions on the disorder-driven superconductor-insulator transition *Physical Review B* **89** 035149
- [10] Osofsky M S, Krowne C M, Charipar K M, Bussmann K, Chervin C N, Pala I R and Rolison D R 2016 Disordered RuO2 exhibits two dimensional, low-mobility transport and a metal–insulator transition *Scientific Reports* **6** 21836
- [11] Kovaleva N N, Chvostova D, Bagdinov A V, Petrova M G, Demikhov E I, Pudonin F A and Dejneka A 2015 Interplay of electron correlations and localization in disordered β-tantalum films: Evidence from dc transport and spectroscopic ellipsometry study *Applied Physics Letters* **106** 051907
- [12] Anderson P W 1959 Theory of dirty superconductors *Journal of Physics and Chemistry of Solids* 11 26-30
- [13] Goldman A M and Marković N 1998 Superconductor-Insulator Transitions in the Two-Dimensional Limit *Print edition* **51** 39
- [14] Hertel G, Bishop D J, Spencer E G, Rowell J M and Dynes R C 1983 Tunneling and Transport Measurements at the Metal-Insulator Transition of Amorphous Nb: Si *Physical Review Letters* **50** 743-6
- [15] Dynes R C, Garno J P, Hertel G B and Orlando T P 1984 Tunneling Study of Superconductivity near the Metal-Insulator Transition *Physical Review Letters* **53** 2437-40
- [16] Yize Stephanie L 2015 Signature of Cooper pairs in the non-superconducting phases of amorphous superconducting tantalum films *Superconductor Science and Technology* **28** 025002
- [17] Sambandamurthy G, Engel L W, Johansson A, Peled E and Shahar D 2005 Experimental Evidence for a Collective Insulating State in Two-Dimensional Superconductors *Physical Review Letters* **94** 017003
- [18] Baturina T I, Mironov A Y, Vinokur V M, Baklanov M R and Strunk C 2007 Localized Superconductivity in the Quantum-Critical Region of the Disorder-Driven Superconductor-Insulator Transition in TiN Thin Films *Physical Review Letters* **99** 257003
- [19] Graybeal J M and Beasley M R 1984 Localization and interaction effects in ultrathin amorphous superconducting films *Physical Review B* **29** 4167-9
- [20] Lee S J and Ketterson J B 1990 Critical sheet resistance for the suppression of superconductivity in thin Mo-C films *Physical Review Letters* **64** 3078-81
- [21] Crauste O, Couëdo F, Bergé L, Marrache-Kikuchi C A and Dumoulin L 2014 Destruction of superconductivity in disordered materials: A dimensional crossover *Physical Review B* **90** 060203
- [22] Gornyi I V, Mirlin A D and Polyakov D G 2005 Interacting Electrons in Disordered Wires: Anderson Localization and Low-T Transport *Physical Review Letters* **95** 206603
- [23] Oganesyan V and Huse D A 2007 Localization of interacting fermions at high temperature *Physical Review B* **75** 155111
- [24] Anderson P W 1958 Absence of Diffusion in Certain Random Lattices *Physical Review* **109** 1492-505
- [25] McMillan W L 1981 Scaling theory of the metal-insulator transition in amorphous materials *Physical Review B* **24** 2739-43
- [26] Crow J E, Strongin M, Thompson R S and Kammerer O F 1969 The superconducting transition temperatures of disordered Nb, W, and Mo films *Physics Letters A* **30** 161-2
- [27] Collver M M and Hammond R H 1973 Superconductivity in "Amorphous" Transition-Metal Alloy Films *Physical Review Letters* **30** 92-5

- [28] Matsuo S, Sugiura H and Noguchi S 1974 Superconducting transition temperature of aluminum, indium, and lead fine particles *J Low Temp Phys* **15** 481-90
- [29] Abeles B, Cohen R W and Cullen G W 1966 Enhancement of Superconductivity in Metal Films *Physical Review Letters* **17** 632-4
- [30] Bose S, Raychaudhuri P, Banerjee R, Vasa P and Ayyub P 2005 Mechanism of the Size Dependence of the Superconducting Transition of Nanostructured Nb *Physical Review Letters* **95** 147003
- [31] Li W H, Yang C C, Tsao F C and Lee K C 2003 Quantum size effects on the superconducting parameters of zero-dimensional Pb nanoparticles *Physical Review B* **68** 184507
- [32] Hein R A, Gibson J W, Pablo M R and Blaugher R D 1963 Critical Magnetic Fields of Superconducting Molybdenum *Physical Review* **129** 136-7
- [33] Rorer D C, Onn D G and Meyer H 1965 Thermodynamic Properties of Molybdenum in Its Superconducting and Normal State *Physical Review* **138** A1661-A8
- [34] Waleh A and Zebouni N H 1971 Study of Supercooling and Thermal Conductivity in Superconducting Molybdenum *Physical Review B* **4** 2977-87
- [35] Mallon R G and Rorschach H E 1967 Measurements of Magnetization in Superconductive Molybdenum *Physical Review* **158** 418-23
- [36] Fàbrega L, Camón A, Fernández-Martínez I, Sesé J, Parra-Borderías M, Gil O, González-Arrabal R, Costa-Krämer J L and Briones F 2011 Size and dimensionality effects in superconducting Mo thin films *Superconductor Science and Technology* **24** 075014
- [37] Fabrega L, Fernandez-Martinez I, Parra-Borderias M, Gil O, Camon A, Gonzalez-Arrabal R, Sese J, Santiso J, Costa-Kramer J L and Briones F 2009 Effects of Stress and Morphology on the Resistivity and Critical Temperature of Room-Temperature-Sputtered Mo Thin Films *Applied Superconductivity, IEEE Transactions on* **19** 3779-85
- [38] Hirakawa A, Makise K, Kawaguti T and Shinozaki B 2008 Thickness-tuned superconductor—insulator transitions in quench-condensed Mo and MoRu films *Journal of Physics: Condensed Matter* **20** 485206
- [39] Ioffe A F and Regel A R 1960 Non-crystalline, amorphous, and liquid electronic semiconductors *Prog. Semicond.* **4** 237-91
- [40] Sangita B, Rajarshi B, Arda G, Pratap R, Hamish L F and Pushan A 2006 Size induced metal-insulator transition in nanostructured niobium thin films: intra-granular and inter-granular contributions *Journal of Physics: Condensed Matter* **18** 4553
- [41] Van der Pauw L J 1958 A Method of Measuring Specific Resistivity and Hall Effect of Discs of Arbitrary Shape *Philips Research reports* **13** 1-9
- [42] Van der Pauw L J 1959 A Method of Measuring The Resistivity and Hall Coefficient of Lamellae of Arbitrary Shape *Philips Technical Review* **20** 220
- [43] Braun C 2002 Parratt32. (Germany: HMI Berlin)
- [44] Lábár J L 2005 Consistent indexing of a (set of) single crystal SAED pattern(s) with the ProcessDiffraction program *Ultramicroscopy* **103** 237-49
- [45] Ross R G and Hume-Rothery W 1963 High temperature X-ray metallography: I. A new debye-scherrer camera for use at very high temperatures II. A new parafocusing camera III. Applications to the study of chromium, hafnium, molybdenum, rhodium, ruthenium and tungsten *Journal of the Less Common Metals* **5** 258-70
- [46] Banerjee R, Sperling E A, Thompson G B, Fraser H L, Bose S and Ayyub P 2003 Lattice expansion in nanocrystalline niobium thin films *Applied Physics Letters* **82** 4250-2
- [47] Gao P-Y, Kunath W, Gleiter H and Weiss K 1988 The structure of small penta-twinned gold particles *Scripta Metallurgica* **22** 683-6
- [48] Schneider C A, Rasband W S and Eliceiri K W 2012 NIH Image to ImageJ: 25 years of image analysis *Nat Meth* **9** 671-5
- [49] Czack G, Kirschstein G, Haase V, Fleischmann W D and Gras D 2013 *Mo Molybdenum: Physical Properties, Part 2. Electrochemistry*: Springer Berlin Heidelberg)

- [50] Koepke R and Bergmann G 1976 The upper critical magnetic field Bc2(T) of amorphous molybdenum films *Solid State Communications* **19** 435-7
- [51] Möbius A, Frenzel C, Thielsch R, Rosenbaum R, Adkins C J, Schreiber M, Bauer H D, Grötzschel R, Hoffmann V, Krieg T, Matz N, Vinzelberg H and Witcomb M 1999 Metal-insulator transition in amorphous Si_{1-x}Ni_x: Evidence for Mott's minimum metallic conductivity *Physical Review B* **60** 14209-23
- [52] Möbius A 1989 Comment on `Critical behavior of the zero-temperature conductivity in compensated silicon, Si:(P,B)" *Physical Review B* **40** 4194-5
- [53] Mani A, Bharathi A and Hariharan Y 2001 Pressure-induced insulator-metal transition of localized states in FeSi_{1-X}Ge_X *Physical Review B* **63** 115103
- [54] Lee P A and Ramakrishnan T V 1985 Disordered electronic systems *Reviews of Modern Physics* **57** 287-337
- [55] Osofsky M, Tardy H, LaMadrid M and Mochel J M 1985 Strong and weak electron spin-orbit scattering near the metal-insulator transition *Physical Review B* **31** 4715-7